5

Analysis of Membrane Protein Stability in *Diabetes Insipidus*

Florian Heinke, Anne Tuukkanen and Dirk Labudde
University of Applied Sciences Mittweida
Germany

1. Introduction

Diabetes insipidus (DI) is a rare endocrine disorder, with an incidence in the general population assessed on one case per 25,000-30,000 people (Robertson, 1995; Ananthakrishnan, 2009; Krysiak, et al., 2010). It is a disease characterized by polyuria and compensatory polydipsia. The underlying causes of DI are diverse and can be central **defects**, in which no functional arginine-vasopressin is released from the pituitary, or may becaused by defects in the kidney (nephrogenic DI, NDI). Four different types of NDI are known. First, acquired NDI can originate as a side-effect of drugs, with the most prominent being the antibipolar drug lithium. Second and third, autosomal recessive and dominant inheritable NDI, are caused by gene mutations in the AQP2 gene encoding aquaporin-2. Finally, mutations in the AVPR2 gene (Deen et al., 1994; Mulders, 1998), which encodes the V2 vasopressin receptor (V2R), are the cause of the X-linked inheritable form of NDI (Fig. 1 right) (Van den Ouweland et al., 1992; Rosenthal, 1992).

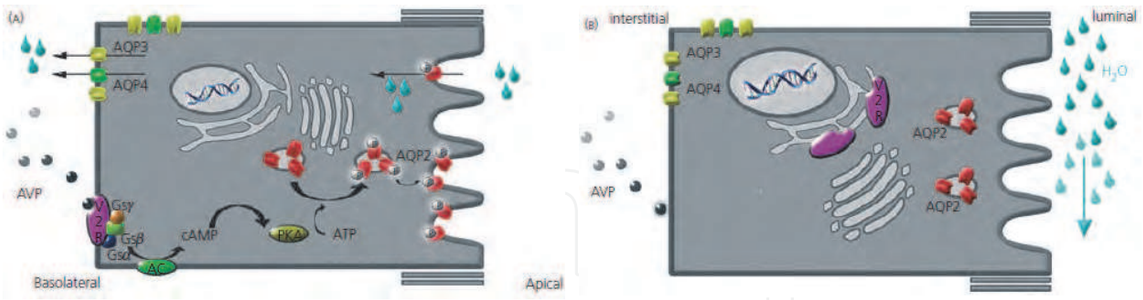

Fig. 1. Transcellular water transport in renal collecting principal duct cells and molecular cause of X-linked nephrogenic diabetes insipidus (NDI)

(Left) Vasopressin binding to its type 2 receptor (V2R) triggers a cAMP cascade that leads to the insertion of aquaporin-2 water channels in the apical membrane. This allows water to pass through this membrane and transcellular water transport to balance concentration of the pro-urine and, there by antidiuresis. (Right) In the X-linked form, NDI is often caused by V2R mutants trapped in the endoplasmic reticulum as a result of their misfolding, making them unavailable for binding arginine-vasopressin (AVP) at the basolateral plasma membrane. As a result, no transcellular water transport takes place, leading to polyuria (Los et al., 2010).

The X-linked inheritable form of nephrogenic diabetes insipidus is a disorder in which patients are unable to concentrate their urine despite the presence of the hormone arginine-vasopressin (AVP). This antidiuretic hormone regulates the process of the water reabsorption, according to the body's need, from the pro-urine that is formed by ultrafiltration in the kidney. It binds to its type 2 receptor in the kidney (Fig. 1, A). Mutations in the gene encoding the V2R often lead to NDI. Many of these mutations do not interfere with the intrinsic functionality of V2R, but cause its retention in the endoplasmic reticulum (ER) making it unavailable for AVP binding.

As a consequence of the inability of the kidneys to concentrate the pro-urine in response to AVP, diseased adult patients may have a daily output of 15–20 l of highly dilute (usually < 100 mOsmol / kg) urine. In newborn infants, NDI is characterized by irritability, poor feeding, poor weight gain and dehydration symptoms.

Classically, the diagnosis NDI was made after a dehydration test (Los et al., 2010) but it has become possible in clinical practice to apply direct analysis of the arginine vasopressin V2 receptor gene (AVPR2) and the aquaporin-2 gene for the diagnosis and differential diagnosis of nephrogenic diabetes insipidus (Fujiwara & Bichet, 2005).

To date, over 200 mutations have been described in the AVPR2 gene, which can be categorized into classes according to their cellular fate (Robben et al. 2006).

Another gene for the diagnosis of **Diabetes insipidus** is WFS1. It encodes a transmembrane protein which induces the Wolfram Syndrom (Hardy et al. 1999), a rare autosomal recessive disorder characterized by juvenile-onset non-autoimmune Diabetes mellitus, optic atrophy, sensorineural deafness and **Diabetes insipidus** (Wolfram & Wagener, 1938). In addition, psychiatric illnesses such as depression and impulsive behavior are frequently observed in affected individuals (Swift & Swift, 2001).

The minimal criteria for diagnosis are Diabetes mellitus and optic atrophy. **Diabetes insipidus**, sensorineural deafness, urinary tract anatomy, ataxia, peripheral neuropathy, mental retardation and psychiatric illness are additional symptoms seen in the majority of patients (Strom, 1998a).

The WFS1 protein, also called wolframin, consists of 890 amino acids and was predicted to have nine or ten membrane spanning domains (Inoue et al., 1998; Strom et al., 1998b). More than 100 mutations of the WFS1 gene have been identified to date in Wolfram syndrome patients. Most are inactivating mutations, suggesting loss of function to be responsible for the disease phenotype (Cryns et al., 2003). The WFS1 protein is expressed in various tissues but at higher levels in the brain, heart, lung and pancreas (Inoue et al., 1998; Strom et al., 1998b). The literature shows that the WFS1 protein is to be localized predominantly in the endoplasmic reticulum and suggested a possible role of this protein in membrane trafficking, protein processing and/or regulation of cellular calcium homeostasis (Takeda et al, 2001). A recent study showed this protein to contain nine transmembrane domains and to be embedded in the ER membrane with the amino-terminus in the cytosol and the carboxy-terminus in the ER lumen (Hofmann et al., 2003).

The short introduction shows the correlation of **Diabetes insipidus** with mutations in different membrane proteins. Membrane proteins play essential roles in cellular processes. Despite the central importance of transmembrane proteins, the number of high-resolution structures remains small due to the practical difficulties in crystalizing them. Many human disease-linked point mutations occur in transmembrane proteins. These mutations cause structural instabilities in a transmembrane protein leading it to unfold or missfold in an alternative conformation.

However, the analysis of this stability plays an important part concerning the understanding process of these diseases, especially for **Diabetes insipidus.** In this chapter, we demonstrate two different approaches on membrane protein stability analysis, results from single-molecule force spectroscopy (SMFS) on aquaporin-1 and a new method based on so called energy profiles.

2. Description of the investigated membrane proteins

The points of interest in this work are the membrane proteins: aquaporins -2, -3 and -4 as well as the arginine vasopressin V2 receptor.

2.1 Aquaporins

For a better understanding of the relationship between mutations and changes in the stability of membrane proteins, we summarize in this section the structural characteristics of water cannels. Knowledge of these aquaporins derived by experimental data revealed the affiliation of aquaporins to a family of related water channels from many species. Aquaporins provide highly permeable pores for water to cross membranes. Four identical subunits form a stable tetramer in the plane of membrane. Each subunit has a narrow pore that is selective for water passing through the middle of a bundle of α-helices. About 10 water molecules line up in a pore about 0.3 nm in diameter. Hydrophobic bonding of water with a pair of asparagine residues (Fig. 2: Asn 76 and Asn 192, human aquaporin-1 numbering) at a narrow point in the pore allows the channel to be selective for water. The monomers of the protein arose by gene duplication, since their sequences are remarkably similar. Various human tissues express 12 different aquaporin isoforms. Aquaporin-1 (Fig. 2) is found in red blood cells, retinal proximal tubules, blood vessel endothelial cells, and the choroid plexus. Aquaporin-2 is required for renal collecting ducts to reabsorb water (King et al. 2004).

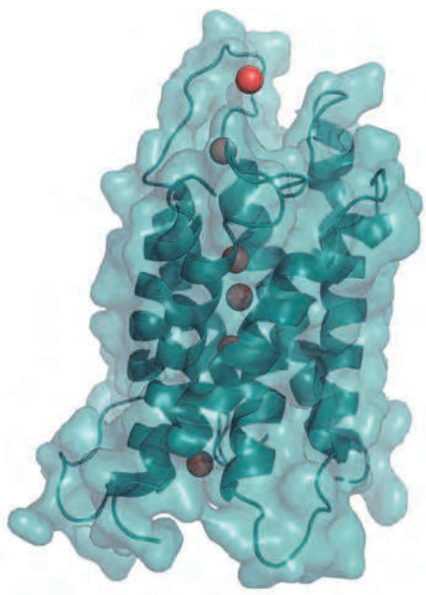

Fig. 2. Structure of an aquaprin-1 protein (PDB_ID 1ih5); The lined up water molecules are shown in red. The protein structure contains seven α-helices.

Antidiuretic hormone controls the insertion of aquaporin-2 in the collecting duct membrane. It activates a seven-helix receptor, causing cytoplasmic vesicles storing aquaporin-2 to fuse with the plasma membrane. This increases the permeability of apical plasma membranes to water, allowing it to move from the urine into the hypertonic extracellular space of the renal medulla. The water selectivity can appreciate by the protein structure. The figure 3 illustrates the network of the involved residues in the process. Additional to the exposed residue pair (Asn 76 and Asn 192) we observed Arg 195 and His 180 on the top of the pore, both closing the pore for bigger molecules or ions. The pore is hydrophobic inside. The peptide bonds of the residues Gly 188 and Ile 191 can form h-bonds with water molecules. The reaction of sensitive Cys 189 with mercuric ions closes the water pore (King et al. 2004; Pollard & Earnshaw, 2007).

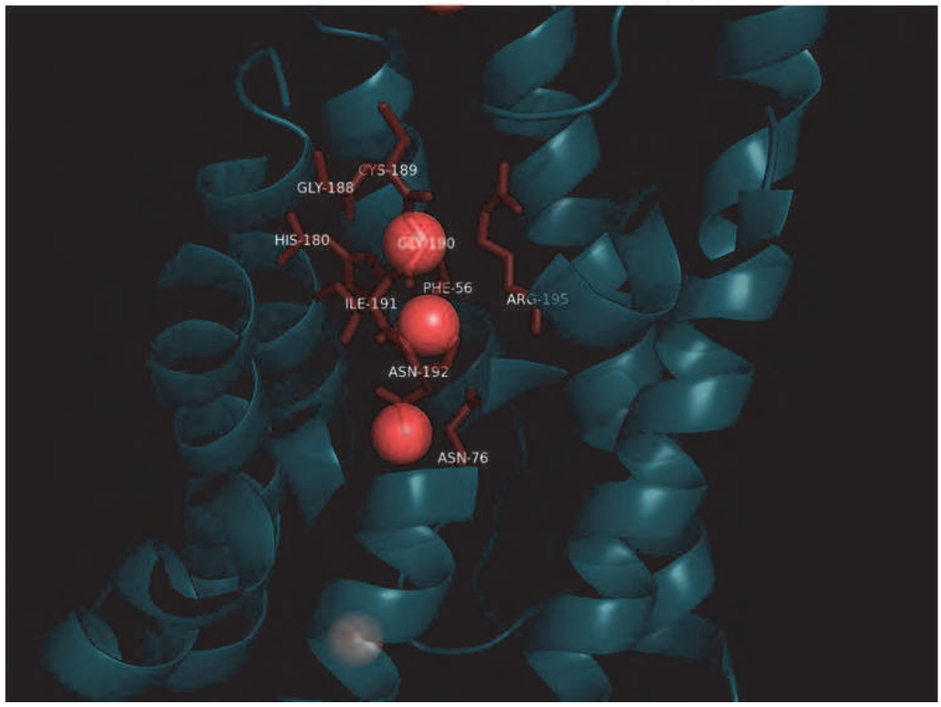

Fig. 3. Aquaporin 1 and the residue network for water transport. The following residues are involved: His 180, Gly 188, Cys 189, Gly 190, Ile 191, Asn 192, Arg 195 and Phe 56, Asn 76.

Furthermore, it is shown that two of the seven helices hold a highly conserved Asn-Pro-Ala motif (Chen et al., 2006). These two motifs meet in opposite α-helical orientation. This conformation induces a bipolar electric field changing the water molecule orientation and preventing protons to move through the channel. Further molecular simulation study has revealed a secondary free energy-barrier induced by Phe 56, His 180 and Arg 195. This barrier is located at the extracellular side, about 8 Å apart from the bipolar field. It forms a constriction region with a diameter of approximately 2 Å which allows only a single water molecule to pass the pore. Thus, the secondary free-energy barrier plays a main role in transport selectivity. Additionally, molecular dynamics simulation of Arg 195 mutants showed a significant decrease of the secondary energy-barrier leading to the loss of selectivity. This indicates that conformational changes or mutations of Arg 195 have a main influence on the transport behavior of aquaporin (de Groot et al. 2004; Chakrabarti et al., 2004a; Chakrabarti et al., 2004b; Ilan et. al, 2004).

The focus of this chapter is the analyses of the stability of membrane proteins. To collect a reliable dataset and to gather information about existing protein structures, we checked the Protein Data Bank (PDB) and the ModBase for aquaporin entries. Table 1 and table 2 give an overview over the used structures for all future calculations and discussions of the aquaporins.

Aquaporin (PDB_ID)	Sequence length (PDB)	Sequence length (Uniprot)	Number missing residues N-terminal	Number missing residues C-terminal	Coverage [%]
Aqp1/1fqy	230	273	7	36	84
Aqp4/3gd8	227	328	31	70	69
Aqp5/3d9s	251	269	1	17	93

Table 1. Overview of aquaporin structure

Aquaporin	BLAST-hit in PDB	e-Value	Model	Model-Template	reliability	Sequence identity
Aqp2:	3d9sA	2.00E-99	x	3d9sA	good	68%
Aqp3:	**1ldfA**	2.00E-46	x	3ldfA	average	43%

Table 2. Overview of models in the ModBase for the structural unknown aquaporin proteins. The highlighted (bold) PDB_ID 1ldf is the structure of a glycerol channel from *E.coli*.

While the structures of aquaporin-1, -4 and -5 have been clarified by electron crystallography (aquaporin-1) or x-ray diffraction (aquaporin-4 and -5) respectively, the structures of aquaporin-2 and -3 have been predicted by homology modeling. In homology modeling, the sequence of a structural unknown protein is queried to a protein structure database (such as the Protein Data Bank or Protein Data Bank of Transmembrane Proteins). The structure with adequate sequence identity (usually greater than 25-30%, depending on the length of the query sequence) is used as the modeling template. By simulations with force fields, using rotamer libraries and machine learning techniques, the query sequence is modeled into the given structure template and the resulting model can be evaluated. Unsuccessful modeling is caused by low sequence identity and leads to short modeled fragments or no model at all. Many of those successfully modeled structures are stored and organized in protein model databases (*e.g.* Modbase and Protein Model Portal). Because of the relatively low number of known structures finding an appropriate template is still a bottleneck in structure homology modeling.

As seen in table 2, the structure model of aquaporin-2 has been produced by using the structure of aquaporin-5 as modeling template. The most reliable structure of aquaporin-3 was modeled on the basis of a glycerol channel of *E. coli*. The neighbor joining tree (see figure 4) of aquaporin 1-5 and the glycerol channel gives insight to sequence similarity of the involved proteins and, in case of aquaporin-2 and -3 their modeling template sequences. As seen by branch length, aquaporin-2 and aquaporin-5 share the highest sequence identity in the entire tree which confirms the applicability of the aquaporin-5 structure of modeling a high reliable aquaporin-2 structure. Aquaporin-3 and the glycerol channel form a single isolated monophyletic cluster with a branch length of about 600 indicating the moderate sequence identity of 43% given in table 2. However, this sequence identity is high enough for deriving a model with an average reliability.

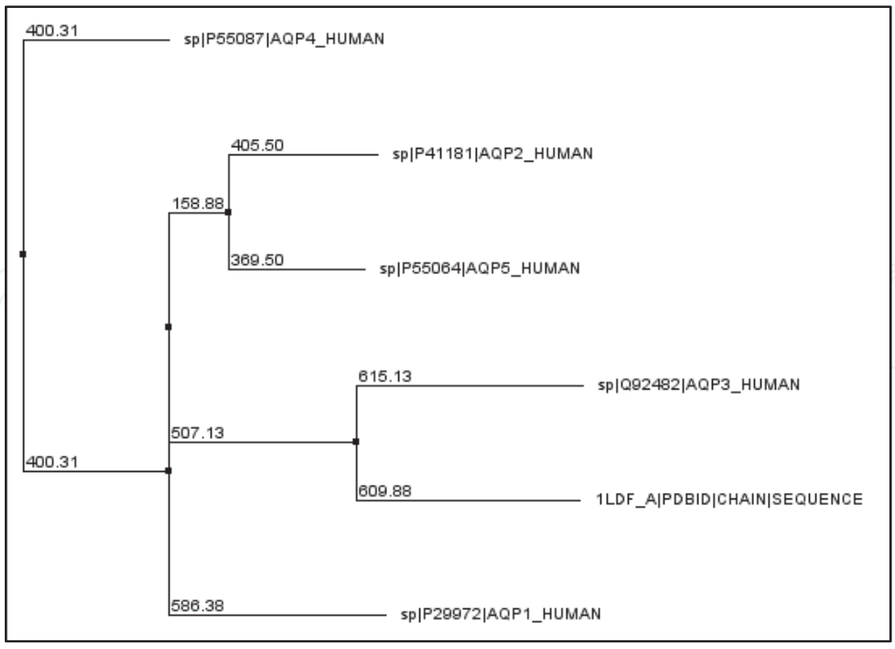

Fig. 4. The neighbor joining tree of aquaporin 1-5 and the glycerol channel of *E. coli* (PDB_ID 1ldf) indicates the sequence similarities of aquaporin-2,-3 and their modeling templates aquaporin-5 and 1ldf, respectively. The direct neighborhood of the involved proteins and their template structures point to the adequate reliability of the existing aquaporin-2 and aquaporin-3 models.

Mutations in aquaporin are correlated with NDI. For the detailed analyses of mutations in aquaporin-2, we concentrated on two well-defined point mutations. Characterization of D150E and G196D aquaporin-2 mutations are responsible for nephrogenic diabetes insipidus: importance of a mild phenotype. These two mutations were compared with the wild-type protein (aquaporin-2-wt) for functional activity (water flux analysis), protein maturation, and plasma membrane targeting. As shown by Guyon et al (2009) the D150E mutant induces an intermediate water flux compared to the aquaporin-2 –wt whereas the G196D mutant leads to no water flux. This observation is consistent with results from immunocytochemical experiments and Western blotting which indicate partial targeting of D105E in plasma membrane and complete sequestration of G196D within intracellular compartments. When coinjecting aquaporin-2-wt with mutants, no (aquaporin-2-wt + D150E) or partial (aquaporin-2-wt + G196D) reduction of water flux were observed compared with aquaporin-2-wt alone, whereas complete loss of function was found when both mutants were coinjected (Guyon, et al., 2009).

2.2 Model of V2 receptor

The V2 receptor belongs to the class A of G-protein-coupled receptors containing seven membrane spanning helices which are connected by extracellular and intracellular loops of varying length. The function of V2R is coupled to the G-protein activating adenyl cyclase (Barberis et al. 1998). If an agonist arginine vasopressin binds to V2R, the receptor becomes activated which leads to allosteric structural rearrangements. These structural changes then enable interactions with the cytosolic G-protein. The binding site of arginine vasopressin on

the V2 receptor is formed within the transmembrane helices II –VII (Slusarz et al. 2006). Regions between residues 88-96, 119-127, 284-291 and 311-317 contain most of the residues involved in binding. The selectivity of vasopressin was proposed to be connected with non-conserved residue Q180 whose carboxamide forms hydrogen bonds with carboxamide of Asn5 in the peptide. The stability of the hormone in the bound state is ensured by two hydrogen bonds between peptide backbone atoms of Tyr 2 and Asn 5. In general, hydrogen bonding and salt bridges were identified as the most important interactions contribution to the arginine vasopressin binding (Slusarz et al. 2006). Significant hydrophobic interactions were not detected.

A three-dimensional structural model of human V2 receptor (Fig. 5) was produced using I-TASSER protein structure modeling pipeline (Roy et al. 2010). I-TASSER builds protein models using multiple threading alignments on template structures and iterative assembly. The top three structural templates used in the structure prediction were PDB_ID 2ks9 (Substance-P receptor) with sequence identity of 19 %, PDB_ID 2rh1 (B2-adrenergic G protein-coupled receptor) with sequence identity of 22 % and PDB_ID 1l9h (bovine rhodopsin) with sequence identity of 18 % to VR2 receptor. The modeled structure was subjected first to conjugate gradient minimization and then MD simulation using the program NAMD2 (Phillips et al. 2005) and the CHARMM27 force-field (MacKerrel et al. 1998). The TIP3P solvent model represented the water molecules (Joergensen et al. 1983). Simulations assumed constant particle number, constant pressure and constant temperature (*NpT*) ensembles. *Langevin* dynamics was used to maintain constant temperature and pressure was controlled using a hybrid *Nose-Hoover Langevin* piston method. Extensive molecular dynamics simulations were done on the modeled structure in order to study its quality and structural stability. The average root-mean-square-deviation of the backbone atoms of the modeled structure during the simulation was found to be 2.7 Å. The model structure has seven helical segments: helix I 34 -64, helix II 73 – 101, helix III 109 – 142, helix IV 153-175, helix V 202-230, helix VI 248-296, helix VII 304-328.

Molecular dynamics (MD) simulation is one of the most common methods to study computationally protein function, conformational flexibility, and interactions. It is a technique to calculate the equilibrium and transport properties of a classical many-body system (Frenkel, 2002). In MD simulations, particles obey the laws of classical mechanics and the technique show how the system of particles evolves in time. The first MD simulation of a protein was done in the 1970s in vacuum for duration of 10ps (McCammon et al. 1977). Nowadays, the computational power allows simulation of about one million atoms, up to 100 Å in size and time scale up to 1 microsecond. Even single membrane proteins in the native lipid environment can be studied. Simulations of large biomolecular systems are becoming more feasible as demonstrated by the work on the MD-based structure prediction of the ribosome complex from *E. coli* (Villa, 2009), the simulation of the assembly of lipids and proteins into lipoprotein particles (Shih, 2007), the MD studies of viral capsid self-assembly (Freddolino, 2006; Miao, 2010) and vesicle fusion simulations (Kasson, 2010). MD simulations are used to gain information about the conformational changes of protein structure, *i.e.* sample the configuration space. In addition, MD simulations provide thermal averages of molecular properties such as the free energy change upon binding or atomic mean square fluctuation amplitudes. According to the ergodic hypothesis all microstates of a system are equally probable for a particle over a long period of time. Hence, the average of a process parameter over time and the average over the statistical ensemble are the equal. Simulation can be used to study the dynamics of a

system in detail by observing the conformational states that are accessible in a given temperature. *Ab initio* structure prediction starting from amino acid sequence of a protein using MD simulations is computationally feasible only for very small proteins, but simulations can be used to improve computational predicted protein structures obtained by homology modeling or fold recognition. The limitations of MD simulations are still relatively short time scale, inaccuracies in the description of physical interactions and the size limitation of the simulation system.

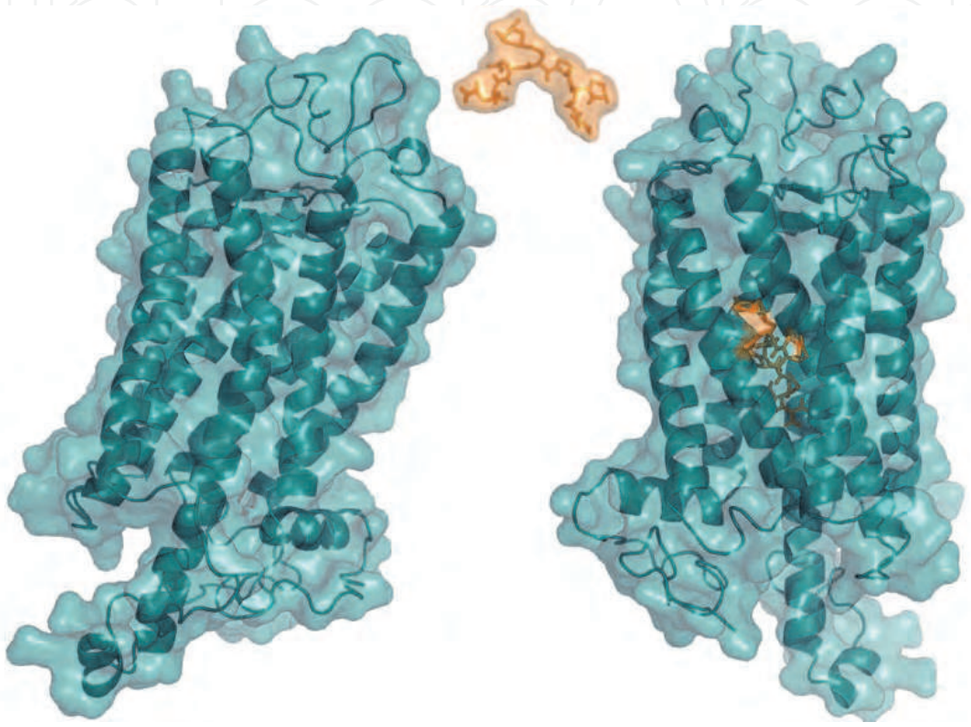

Fig. 5. Structure model of the V2 receptor (left). On the right side a result from Molecular Docking Server. The AVP hormone is highlighted in orange and is bound to the V2 receptor (right).

Mutation	Effect
A84D	This mutation not only affects receptor folding in such a way as to lead to its retention inside the intracellular compartments but, as expected, also has profound effects on its binding and coupling properties (pubmed_Id 10820167).
I130F	Functional analysis of I46K and I130F revealed reduced maximum agonist-induced cAMP responses as a result of an improper cell surface targeting (pubmed_Id 10770218,16006591)
P322S	P322S mutation of AVPR2 gene leads to a mild form of CNDI. (pubmed_Id 10026830,9402087)

Table 3. Overview of mutations in the V2 receptor and a short description of the biological effect. (More mutants in the appendix.)

In this work we address only a repertory. We do not analyses mutations cause constitutive activation of the receptor in this work (such as: Feldman et al, 2005). The table 3 shows the position and the molecular description of the investigated mutations of the V2 receptor be focused on this work.

3. SMFS – Stability and experiments

Atomic force microscopy (AFM) is mostly known for its imaging capabilities (Müller & Engel, 1999; Müller, et al, 1999; Seelert et.al, 2003). Recently, single-molecule force spectroscopy (SMFS) has proven to be a tool for detecting and locating inter- and intra-molecular forces on a single molecule level. SMFS experiments allow measuring the stability of membrane proteins and also probing the energy landscapes (Janshoff et al., 2000; Janovjak et al, 2004). In Fig. 6A a schematic representation of the force spectroscopy instrumentation is shown. Molecules with complex three-dimensional structures, such as proteins, can be unfolded in a controlled way. When transmembrane proteins are unfolded in force spectroscopy experiments, during continuous stretching of the molecule the applied force is

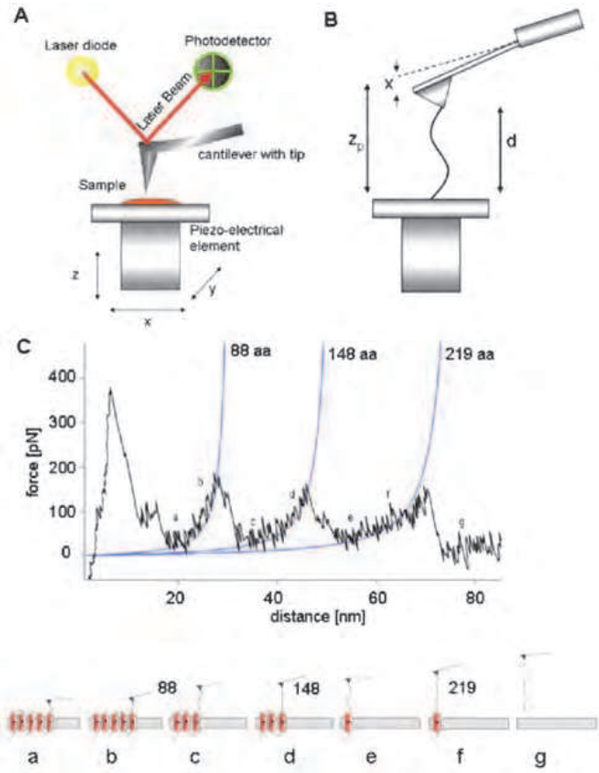

Fig. 6. A: Schematic representation of AFM. The sample is mounted on a piezo-electric element and scanned under a sharp tip attached to the cantilever. The voltage difference of the photodetector is proportional to the deflection of the cantilever.
B: Unfolding of a transmembrane protein. A single molecule is attached between the tip and the sample while the distance between tip and sample is continuously increased.
C: Typical spectrum obtained from an unfolding experiment of bR with the main peaks fitted by a hyperbolic function (WLC model) and correlated to the unfolding of secondary structure elements (cartoon at the bottom).

measured by the deflection of the cantilever and plotted against extension (tip-sample separation), yielding a characteristic force-distance curve (F-D curve) (see Fig. 6). From the analysis of single molecule force spectra it is possible to associate the peaks to individual stable structural segments within membrane proteins. For a given protein under study, the F-D curves exhibit certain patterns, which contain information about the strength and location of molecular forces established within the molecule, stable intermediates and reaction pathways, and the probability with which they occur. For membrane proteins the sequence of the unfolding peaks follow the amino acid sequence of the protein. Fitting each peak to a hyperbolic function, the worm-like chain model (WLC), gives the number of already unfolded amino acids (Rief et al. 1997).

Consequently, with the peaks and the predicted secondary structure, it is possible to associate the peaks to structural domains (see Fig. 7 and Fig. 8). Force curves show specific and unspecific interactions which lead to different unfolding pathways.

To draw biologically relevant conclusions on molecular interactions about how strong they are and where they occur, or whether they are independent or occur only in presence with other events, one must analyze many F-D curves by identical objective procedures. Thus, there is an increasing demand for data analysis techniques that offer fully automated processing of many datasets with identical analysis procedures. To discriminate force spectra showing specific and non-specific interactions and different unfolding/unbinding pathways, classification and pattern recognition algorithms are urgently needed (Marcico et al. 2007; Sapra et al., 2008).

One aim of the analyses of experimental data from SMFS measurements is the detection of possible unfolding pathways. Furthermore, we can identify different groups in hierarchical trees, which relate to different unfolding events. These events correspond to secondary structure elements and stabilized regions in the investigated protein.

3.1 SMFS experiments on aquaporin-1

Here, we work on data from SMFS experiments for human aquaporin-1 from the literature In the work of (Möller et al, 2003) 26 F-D curves were measured and manually aligned. The individual hAQP1 molecules were unfolded by pulling at their C-termini. The author created an overlay of all investigated curves (Fig. 7).

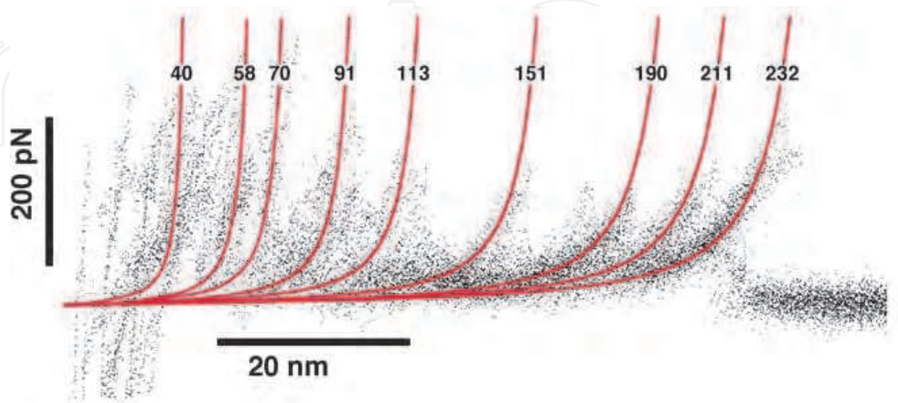

Fig. 7. Overlay of 26 F-D curves of the human aquaporin-2 and fitted using the WLC model (continuous curves). The numbers on the WLC fits indicate the contour lengths used to obtain the fit, in amino acids (Möller et al, 2003).

The next step is the mapping of the unfolding results of the known structure of aquaporin-1. This leads to a correlation of unfolding events and the secondary structure of the membrane protein. A possible description of all events is listed in table 4.

Contour length from WLC fits (aa)	Peak occurrence number/percent (n_{total} = 26)	Average force (pN)	Proposed potential barrier	Grey marker (Fig. 8)
40 ± 8	26 (100%)	206 ± 64	end of helix H6	1
58 ± 6	24 (92%)	157 ± 49	end of helix HE	2
70 ± 8	17 (65%)	125 ± 63	end of helix H5	3
91 ± 7	22 (85%)	156 ± 44	Helix H5	4
113 ± 7	13 (50%)	98 ± 54	end of helix H4	5
151 ± 5	20 (77%)	82 ± 53	Helix H3	6
190 ± 10	17 (65%)	98 ± 33	end of helix HB	7
211 ± 6	16 (62%)	77 ± 42	HelixH2	8
232 ± 5	26 (100%)	152 ± 62	HelixH1	9

Table 4. Contour lengths, peak occurrence, average forces, and positions of potential barriers in Aqp1 topology by SMFS experiments (additional link to Fig. 8 – topology).

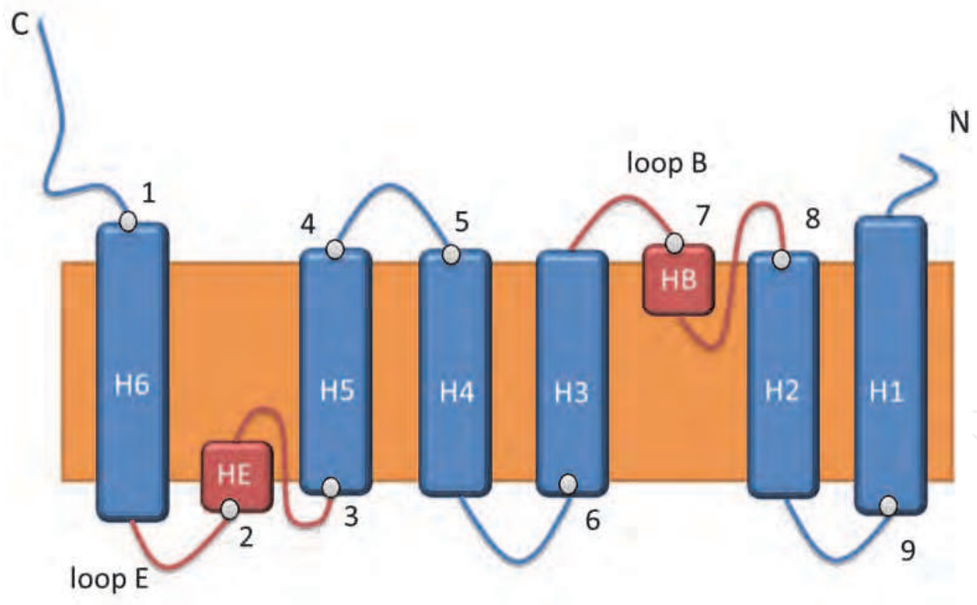

Fig. 8. Topology model of Aqp1: Shown are the secondary structure elements in the lipid bilayer, as described by the 3D structure. Numbers in ovals represent the numbers of proposed potential barrier of table 4.

Interesting are the two long loops, with formed helices in the transmembrane region. A view of the structure of aquaporin-1 quickly shows the role of both helices (HB and HE). The residues Asn 72 (part of HB) and Asn 192 (part of HE) arrange the immediate place of the pore (Fig. 8 and 9).

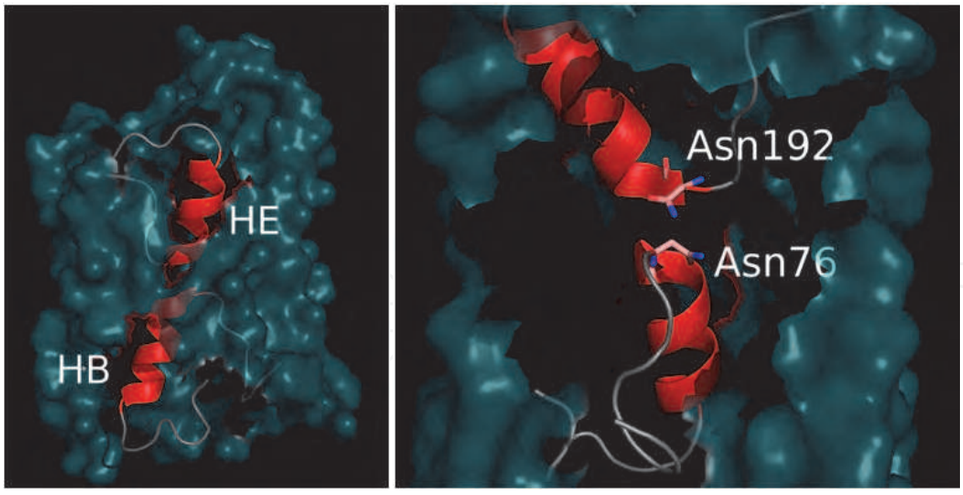

Fig. 9. Structure of aquaporin-1: Left side loop regions E and B (transmembrane helices HE and HB highlighted in red), right: Interface with conserved residues Asn 192 and Asn 76.

This important functional and structural feature corresponds to two unfolding events in aquaporin-1. The major force peak appeared within the noisy region but at a tip–membrane separation of about 20 nm. The WLC fit (Fig. 7 red line – 58 aa) showed an average contour length of 58±6 amino acids, while the rupture event exhibited an average force of 147±49 pN. According to the topology shown in Fig. 8, the extracellular end of helix HE is separated from the C-terminal end. Thus, this adhesion peak is likely to reflect the unfolding of HB. We can observe an analog situation for the loop B and the corresponding helix HB.
The force peaks found at a contour length of 190±10 amino acids (Fig.7) exhibit an average rupture force of 98±33 pN. This distance from the C-terminus corresponds to helix HB, which dips into the membrane from the cytoplasmic side and is only 11 amino acids long. Thus, this adhesion peak is likely to reflect the unfolding of HB.

3.2 Unfolding characteristic of aquaporin-2 and aquaporin-3

On the basis of known structures of aquaporin-1,-4 and -5 and the models of the aquaporin-2 and -3 we created a multiple structure alignment using the PDBeFold service of the EMBL-EBI. We clustered the resulting q-scores of all pair wise structural alignments by applying the UPGMA method (Unweighted Pair Group Method with Arithmetic Mean) to get a rooted tree (see Fig. 10, left). The inner node of the tree indicates that the known structures of aquaporin-5 and the glycerol channel (PDB_ID 1ldf) are almost identical in protein fold. The direct neighborhood of the aquaporin-1 structure and the models of aquaporin-2 and -3 give a strong hint for the unfolding characteristics of aquaporin-2. Due to their high structural similarity we postulate that aquaporin-2,-3 have a similar unfolding characteristic in comparison to aquaporin-1. The pair wise structural alignment of aquaporin-2 and -3 is shown in Fig. 10, right. The structure of aquaporin-4 shares a high similarity to the other structures.

4. Energy profiles – Stability and theory

A lot of tools and methods in the field of bioinformatics and structural biology are based on structure and/or sequence comparison. In this section we demonstrate a new method based on so called energy profiles for analyzing protein structure stability. Those profiles are

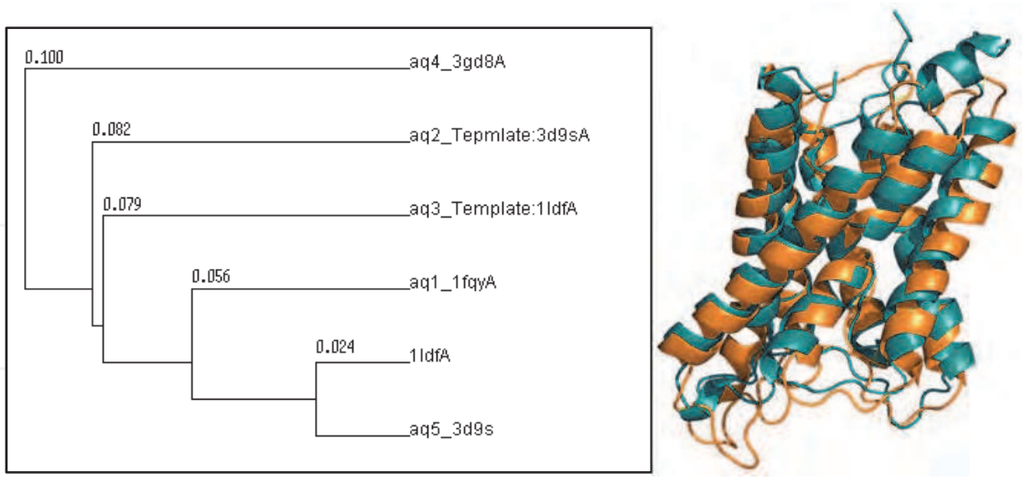

Fig. 10. Left: tree of the q-scores resulting from the PDBeFold service using Unweighted Pair Group Method with Arithmetic Mean (UPGMA) hierarchical clustering. Right: A structural alignment of aquaporin-1 structure (orange) and the model of aquaporin-2 (cyan).

calculated by coarse grained models. Based on the residue contacts in known protein structures, we calculated the potential for pair wise residue-residue-interactions. An energy profile is a schematic plot of the interaction energy of each residue as a function of the residue position in the sequence.

4.1 Theory of energy profiles

In this section, we show the theoretical aspects and calculation of so called protein energy profiles. The aspects explained in this section are essential in understanding the energy profile based methods we applied to the aquaporin proteins.

Energy profiles are derived by coarse-grained amino acid interaction models based on information of known protein structures. In general, the energy of any protein is given by equation (1), where e^*_{ij} acts as the interaction energy between two amino acids a_i and a_j. The function $f(r_{ij})$ quantifies e^*_{ij} by the Euclidean distance r_{ij}. The solvent interaction energy of an amino acid a_i is given by e'_{i0} and is relativized by expression $g(i)$, which describes the solvent accessibility state of a_i.

$$E = \sum_{<ij>} e_{ij} f(r_{ij}) + \sum_{i} e'_{i0} g(i) \tag{1}$$

Based on (1), we designed a coarse grained interaction scheme, which uses the C_α and C_β coordinates of the amino acids. Furthermore we redefined $g(i)$ and $f(r_{ij})$. Instead of using a continuous space, $f(r_{ij})$ acts as Boolean function. That means, depending on r_{ij}, amino acid a_i is either interacting with amino acid a_j or it is not. Based on the work of (Dressel et al. 2007; Wertz & Scheraga, 1978) we defined a cut-off threshold for r_{ij} of 8Å. That leads to the equation (2).

$$f(r_{ij}) = \begin{cases} 1 & \text{if } r_{ij} \text{ is} \leq 8\text{Å}, \\ 0 & \text{else.} \end{cases} \tag{2}$$

ÅFurthermore we introduced an amino acid specific inside/outside-property which reflects the orientation of the amino acid side chains with respect to the center of mass of the neighboring residues and was defined in the following way:
A residue is declared as inside, if

$$\left|\vec{C}_\alpha - \vec{c}\right| < 5 \vee \left(\vec{C}_\alpha - \vec{C}_\beta\right)\left(\vec{C}_\alpha - \vec{c}\right) < 0 \tag{3}$$

$\vec{C}_{\alpha/\beta}$ are the vectors of the $C_{\alpha/\beta}$ atoms, $\vec{c}$ is the center of mass of all amino acids in a surrounding sphere with a radius of 5Å. For determining the center of mass only C_α atoms are taken into account. Using this property the inverse Boltzmann equation can be applied to calculate the energy of each amino acid a_i in the protein structure by (4).

$$e_i = -k_B T \ln\left(\frac{n_{(i,in)}}{n_{(i,out)}}\right) \tag{4}$$

The parameters $n_{(i,in)}$ and $n_{(i,out)}$ are equal to the number of inside and outside occurrences of amino acid a_i, respectively. These parameters are derived by known globular and membrane protein structures. In our coarse grained model, the interaction energy e_{ij} between two amino acids a_i and a_j is equal to the summation of e_i and e_j. Finally, let S be a set of amino acids, let $k = |S|$ and a_i is defined as the observed amino acid. For each $a_j \in S$ is $r_{ij} \leq 8$Å. Then the total energy E_i of a_i equals (5). By iterating over all amino acids in a protein structure the total energy for each amino acid can be calculated and the energy profile is generated.

$$E_i = \sum_{j=1}^{k}\left(e_i + e_j\right) = \sum_{i=1}^{k}\left(-k_B T \ln\left(\frac{n_{(i,in)}}{n_{(i,out)}}\right) - k_B T \ln\left(\frac{n_{(j,in)}}{n_{(j,out)}}\right)\right) \tag{5}$$

Additionally, it needs to be said that we discard further solvent interaction calculation (seen in the second summation in equation 1) because these information is modeled by the amino acid specific inside/outside-property. In addition, we declared T as constant which leads to discarding the constant $-k_B T$ in the energy profile calculation. Thus the energies, which result by our model, are arbitrary unit entities [a.u.] and are direct proportional to energies given in [J] or [kcal·mol^{-1}].
In conclusion, by calculating the total energy of an amino acid in a protein structure, physicochemical and structural information are abstracted to one single value.
The relation of amino acid stability and amino acid energy is explainable by the folding of the protein and its energy landscape. As one of the last steps in protein biosynthesis the polypeptide folds into the native protein structure state spontaneously which is equal to the proteins most stable fold. This process can be described as a function of the loss of the Helmholtz free energy within an amino acid interaction energy state. Commonly a folded protein in its stable state holds the minimized amount of free energy. The energy profile is a transformation of the energy landscape of the protein at the point of minimized free energy, which leads to the conclusion that the energy value of an amino acid a_i given by an energy profile is a transformation of the stability of the amino acid a_i in the structure. Figure 11 illustrates the resulting energy profile (right) of the structure model of aquaporin-2 (left).

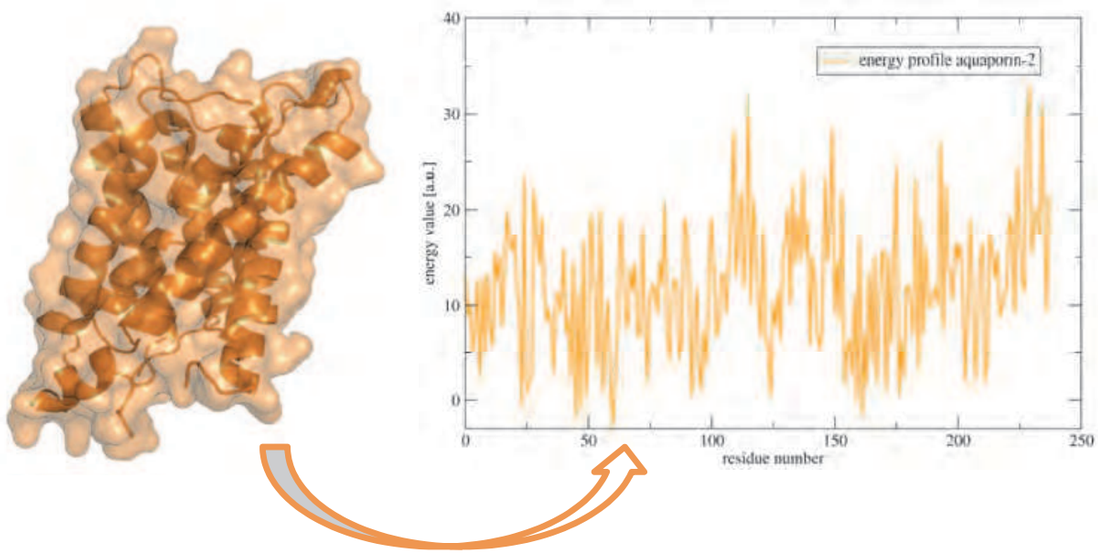

Fig. 11. Left: Structure model of aquaporin-2 and the corresponding energy profile (right) of this model.

4.2 Energy profiles analyses of the investigated aquaporins

On the basis of the so-called energy profiles we can compare the structures and models of all investigated aquaporins, well-defined mutations and the influences of mutations for the stability of the aquaporins.

4.2.1 Energy profiles of the investigated aquaporins

For calculating the energy profiles we used the structures given in table 1 and table 2. To evaluate the energy profiles we checked the already existing aquaporin models concerning their reliability. As shown, the best matching structures were used as template structures for homology modeling. On the level of energy profiles we can confirm our hypothesis that all investigated aquaporins have the same stability characteristics. For this purpose we created a multiple energy profile alignment (MEPAL). We adapted standard algorithms in clustering and deriving consensus profiles and energy conservation. Figure 12 shows the MEPAL for all of the involved aquaporins in **Diabetes Insipidus** and the human aquaporin-1.

The MEPAL method is based on classical multiple sequence alignment algorithms using modified scoring functions optimized for energy profile comparison. The tree (see Fig. 13) is calculated by applying the UPGMA clustering method to the pair wise distance scores which are calculated by the MEPAL algorithm. Furthermore, the graphical alignment output (Figure 12) consists of three parts. The upper row shows the energetically aligned energy profiles represented by the amino acids of the protein sequence which are colored depending on their energy. The greater the energy of an amino acid the greater is the red color content. The middle row shows the consensus profile. In the consensus profile, each energy at position *i* is derived by calculating the pair wise distance sores of all aligned energies at position *i*. The energy with the lowest average distance is representing the consensus profile at position *i*. Finally, the bottom row shows the conservations at each alignment position. Each conservation value is calculated by the sum of pair wise energy distances and is normalized by the number of aligned profiles (Gusfield 1993, Gusfield 1997).

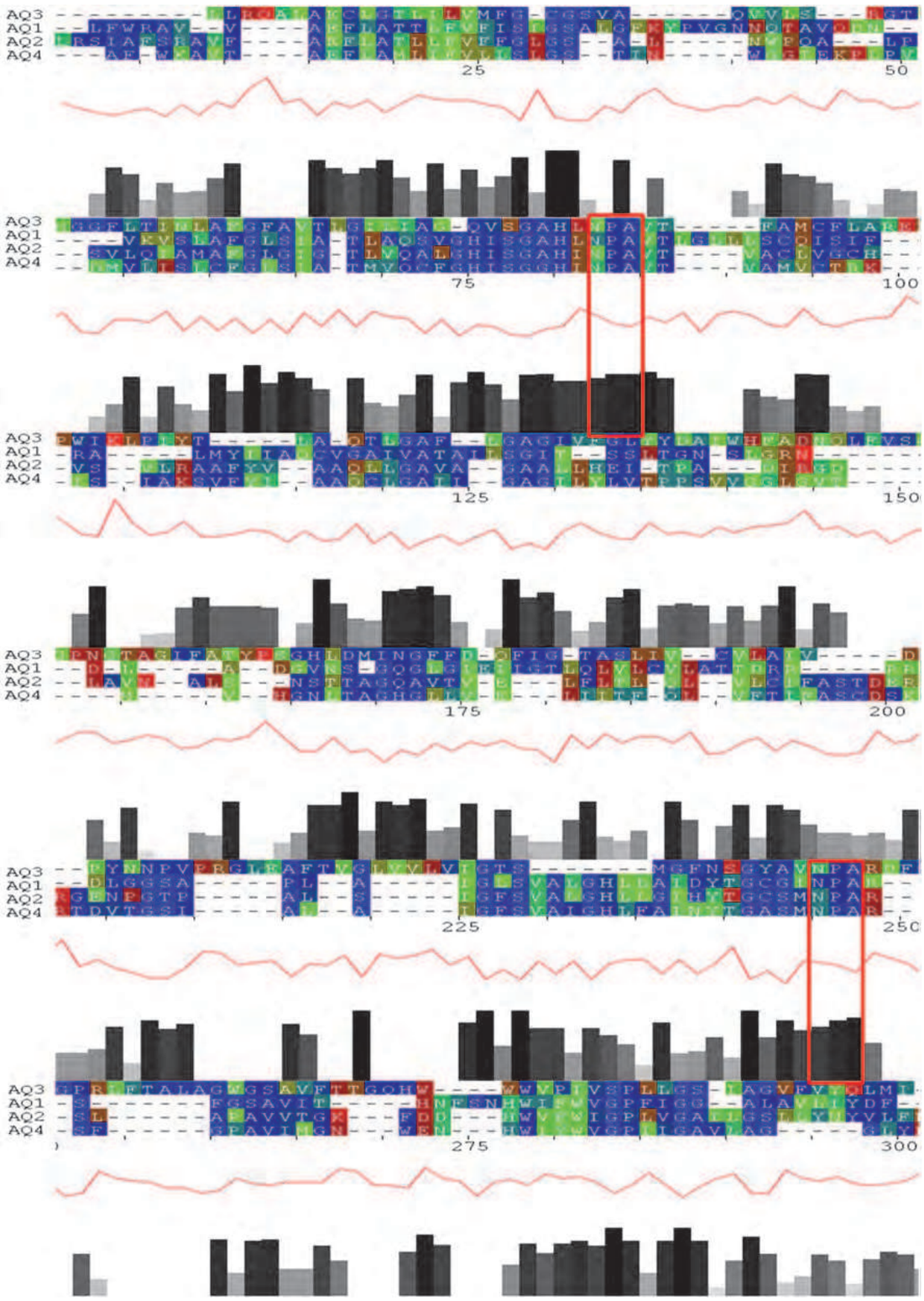

Fig. 12. MEPAL output for the energy profile alignment of aquaporin-1, -2,- 3 and -4. The Asn-Pro-Ala motifs are highlighted by red boxes.

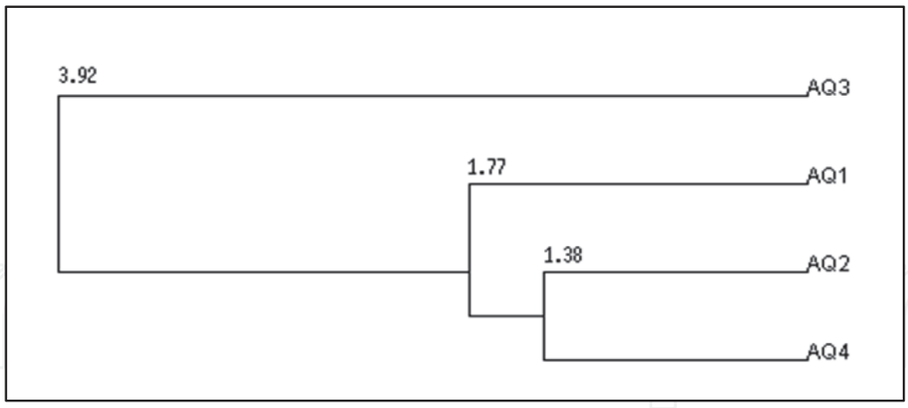

Fig. 13. UPGMA tree, based on energy profiles of aquaporin-1, -2, -3 and -4.

The energy profile alignment based UPGMA Tree, which was calculated by MEPAL indicates high similarities between the energy profiles of aquaporin-1,-2 and -4 and is seen in figure 13. The distance of 3.92 between aquaporin-3 and the other structures corresponds to significant similarity. The graphical output of the MEPAL illustrates several highly energetically conserved amino acids and regions. Two of these conserved regions correspond to the opposite orientated Asn-Pro-Ala motifs in helix HB and helix HE (see section 2.1). These two motifs are highlighted by red boxes in Fig. 12. The energetic conservation of these motifs and their surrounding amino acids confirms the importance of these residues in water transport in aquaporin. Additionally the residues Gly 188, Phe 56, Cys 189, Ile 191 and His 180, which are involved in water transport as well, show differences in sequential and energetic conservation. In detail the conserved amino acids Gly 188 and Phe 56 show slight divergences or no divergences at all concerning their calculated energy. Cys 189 and Ile 191 show no conservation in aquaporin 1-4; but these changes have no effect on the level of energy profiles. Missing in aquaporin-3, His 180 shows sequential and energetic conservation in the other aquaporins. We postulate that these slight divergences do not affect the water flux significantly.

A further point of interest lies in Arg 195. This residue is conserved in all four proteins but varies energetically. These divergences arise from conformational changes of the residue and the structural environment. Based on the facts we referred to in section 2.1, we postulate that these divergences between aquaporin 1-4 lead to a change in the secondary free-energy barrier influencing the transport selectivity and the water flux. It also needs to be said that the significant differences in the energy profile progression between aquaporin-3 and the other structures (see Fig. 13) might result by the less reliable aquaporin-3 model. Despite these divergences, we can confirm our postulated similarities concerning the unfolding characteristics of the aquaporins involved in **Diabetes Insipidus**.

4.2.2 Energy profiles and stability of the mutants of aquaporin-2

For comparison on the level of energy profiles we generated aquaporin-2 models with the two mutations: D150E and G196D. Based on all three models we calculated the energy profiles and created a MEPAL. The results lead to a distance tree and can be discussed on the level of aligned energy profiles (Fig.14).

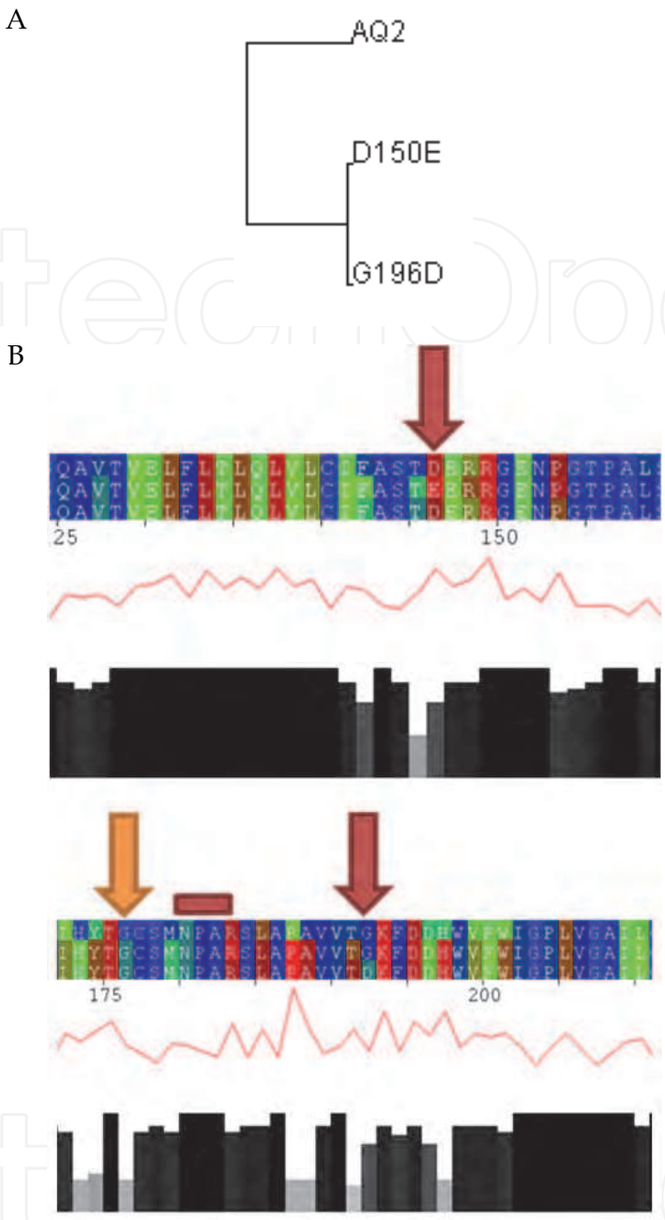

A: The UPGMA tree of the resulting distance scores of the energy profiles calculated by MEPAL. The inner node indicates that these point mutations lead similar energy profiles.
B: The MEPAL output of the investigated energy profiles. The point mutations induce various energetic changes which are highlighted by arrows. The red rectangle illustrates the Asn-Pro-Ala motif.

Fig. 14. Results from the analyses of the energy profile of aquaporin-2 and the investigated mutants.

The energy profile based UPGMA tree (see Fig. 14, A) indicates strong similarities between the energy profiles of the two modelled aquaporin-2 mutants. This leads to the conclusion that both mutants induce the same energetic, structural and functional changes. While both mutations led to energetic variations in the entire energy profiles we focused our discussion on the mutations sites (see Fig. 14, B - red arrows). It needs to be said that because of the

modelling procedure and the energy profile calculation the resulting energy profile covers not all amino acids of the mutated sequence. In this case, this leads to an index indention of 3 amino acids. The mutation D150E (see Fig. 14, B - at the top) induces an energetically increase of the two surrounding residues decreasing the energetic conservation at these positions. Interestingly, in this region the mutation G196D induces almost the same energetic increase as D150E. At the mutation site of the modelled G196D variant (see Fig. 14, B - at the bottom), the mutation induces slight energetic divergences in the region where the mutation site is located. Furthermore, in this region the G196D mutation leads to the same energetic variations as the D150E mutation. This observation can be confirmed at nearly all positions in the energy profiles of the modelled aquaporin mutations. Interestingly, both mutations do not affect the energetic conservation of the Asn-Pro-Ala motif (highlighted by a red rectangle in Fig. 14, B at the bottom).
Additionally, we point to the energetic changes of Gly 188 (highlighted by an orange arrow in 14 B at the bottom). As mentioned in section 2.1 this residue is involved in water transport. Both mutations lead to an energetically increase of Gly 188 and reduce the energetic conservation in these three investigated energy profiles. Thus, we postulate that the mutations D150E and G196D affect the transecullar water transport.

4.3 Energy profiles analyses of the V2 receptor

For investigating energetic influences, binding capabilities and the effect of mutations in the V2 receptor we generated a V2 receptor model by molecular modeling. This model was used to calculate the energy profile of this receptor. Furthermore, we used the Molecular Docking Server to process a docking simulation of the V2 receptor model and the arginine vasopressin hormone. The structure of the model and its hormone in docked state was used for further analyses. Both models are illustrated in Fig. 5 in subsection 2.2. We calculated the energy profile of the V2 receptor model in docked state to detect energetic divergences induced by conformational changes and the hormone itself. Thus, AVP is an oligopeptide it can be integrated into the energy profile calculation in the way it is explained in section 4.1.
To detect docking induced energetic changes both derived energy profiles were aligned using the MEPAL method. The alignment revealed energetic divergences in the surrounding of the amino acids Ala 84 (Fig. 15, A), Ile 130 (Fig. 15, B) and Pro 322 (Fig. 15, C). This leads to the conclusion that these amino acids are involved in hormone binding. Mutations of these amino acids are well described in literature and are causing a loss in functionality and hormone affinity (see table 3). Our novel energy profile based approach brought more evidence to these described mutations.

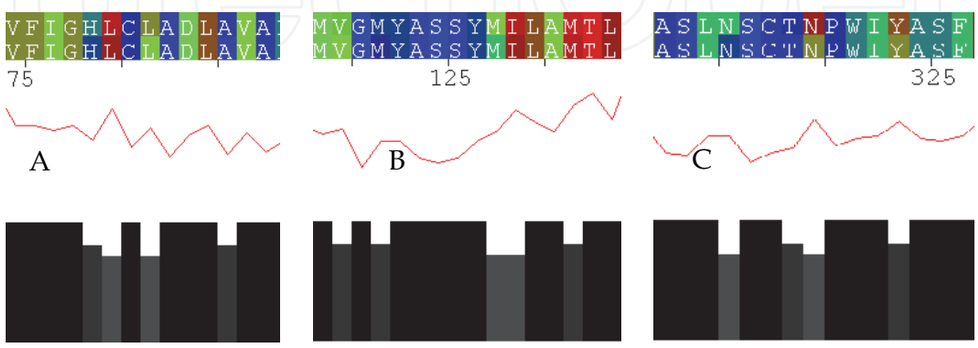

Fig. 15. MEPAL output for the energy profile alignment of fragments of V2 receptor and the complex

5. Discussion of the stability of the investigated membrane proteins

The antidiuretic hormone, ADH, also called vasopressin and arginine-vasopressin, is a nanopeptide (nine amino acids) synthesized in the hypothalamus, transported to and stored in the posterior lobe of the pituitary gland which releases it into the blood circulation. It has antidiuretic and vasopressor actions. The effects of vasopressin result from stimulation of V1 and V2 receptors, V1 mainly responsible for vasoconstriction, V2 for the antidiuretic effect V1 receptors are coupled by G-protein to phospholipase C. V2 receptors are coupled by G-protein to adenylcyclase. Its activation elicits an increase in cAMP which, via protein kinases, induces the activation of aqueous channel aquaporin-2 -mainly located in the renal collecting duct. Under the influence of vasopressin aquaporin-2 migrates from the cytoplasm to the apical membrane. In **nephrogenic diabetes insipidus** there are aquaporin-2 alterations.

Aquaporin-3 is constitutively expressed in the basolateral membrane of the cell. When water floods into the cell through aquaporin-2 channels, it can rapidly exit the cell through the aquaporin-3, 4 channels and flow into blood.

We investigated the stability of membrane proteins on the basis of experimental and theoretical assumptions. Membrane proteins play essential roles in cellular processes. These mutations cause structural instabilities in a transmembrane protein leading it to unfold or missfold in an alternative conformation. By the structural comparison of the aquaporin-1, investigated by SMFS, with the involved proteins and protein models, we can postulate that aquaporin-2,-3 and -4 exhibit similarities in unfolding characteristics. This assumption can be confirmed by our theoretical approach. These theoretical methods are based on the so called energy profile calculation which is explained in this work. On the basis of stability analyses and the application of energy profile based methods we were able to enforce evidence for water flux reduction induced by well described mutations. Furthermore the correlation of residue conservation and energetic conservation of amino acids involved in water transport was detected. Especially the role of the two conserved helices HB and HE could be detected and described on the basis of experimental and theoretical methods.

For analyzing the V2 receptor we derived a structure model by molecular modeling and processed AVP docking simulations. As a main part we focused on selected point mutations and their influences in hormone affinity. Thus, we were able to enforce evidence described in literature.

6. Acknowledgment

This project was funded by the Free State of Saxony and the University of Applied Sciences Mittweida. The authors thank Daniel Stockmann for helpful discussions, motivations and powerful programming.

7. Appendix

In the preparation of the book chapter we collected the literature for well-defined mutations in the V2 receptor. We don't claim to have a complete list or all description. On the basis of this list we compared our results in the context of the docking model of the complex V2 receptor and the AVP hormone.

Mutation	Effect
N22Q	N-linked glycosylation at asparagine 22, Mutagenesis of asparagine 22 to glutamine abolished N-linked glycosylation of the V2 receptor (N22Q-V2R), without altering its function or level of expression. (pubmed_Id 10362843)
L44F	the mutant L44F and the in vitro mutant S167A were expressed in their mature form at wild-type levels (pubmed_Id 8863826)
L44P	mutants L44P, W164S, S167L, and S167T lacked complex glycosylation and were expressed at low levels, mutants misfolded (pubmed_Id 8863826,16006591)
S45C	Strong beta-catenin (CTNNB1) expression in the tumor cells and identified a heterozygote missense Ser45Cys mutation of exon 3 of CTNNB1 (pubmed_Id 19294427).
I46K	Functional analysis of I46K and I130F revealed reduced maximum agonist-induced cAMP responses as a result of an improper cell surface targeting (pubmed_Id 10770218)
L62P	core-glycosylated mutants L62P and V226E were excluded from lysosomes (pubmed_Id 18048502)
A84D	this mutation not only affects receptor folding in such a way as to lead to its retention inside the intracellular compartments but, as expected, also has profound effects on its binding and coupling properties (pubmed_Id 10820167).
A98P	the cell-surface expressions of mutant receptors were totally (A98P and L274P) (pubmed_Id 17371330)
W99R	Mutation of a tryptophan located at the beginning of the first extracellular loop (W99R) that greatly impaired the binding properties of the receptor and had a minor effect on its intracellular routing (pubmed_Id 10820167).
F105V	the F105V mutation is delivered to the cell surface and displayed an unchanged maximum cAMP response, but impaired ligand binding abilities of F105V were reflected in a shifted concentration-response curve toward higher vasopressin concentrations. As the extracellularly located F105 is highly conserved among the vasopressin/oxytocin receptor family, functional analysis of this residue implicates an important role in high affinity agonist binding. (pubmed_Id 10770218)
R113W	The cell-surface expressions of mutant receptors were totally (A98P and L274P) or partially (R113W) absent. V2R-R113W, -G201D, and -T204N were expressed in the ER and in the basolateral membrane as immature, high-mannose glycosylated, and mature complex-glycosylated proteins. The immature forms of V2R-R113W and -T204N, but not V2R-G201D, were rapidly degraded. The mature forms varied extensively in their stability and were degraded by only lysosomes (V2R-T204N and wild-type V2R) or lysosomes and proteasomes (V2R-G201D, -R113W). (pubmed_Id 17371330,16006591,7984150,10770218)

I130F	Functional analysis of I46K and I130F revealed reduced maximum agonist-induced cAMP responses as a result of an improper cell surface targeting (pubmed_Id 10770218,16006591)
R137C	(R137C) in the second intracellular loop, which has been associated with constitutive activation of the AVPR2. In conclusion, adults with intermittent, severe hyponatraemia may have a constitutively activating mutation in the AVPR2 with resultant nephrogenic syndrome of inappropriate antidiuresis. R137C gain-of-function mutation was detected by means of mutation analysis of the V2R gene. (pubmed_Id 18753429,18622631,16843086,19179480,17229917)
R137L	V2R-R137L mutant interacts with beta-arrestins in an agonist-independent manner resulting in dynamin-dependent internalization. V2R-R137L mutant traffic considerably more efficiently to the plasma membrane than V2R-R137H, identifying this as a potentially important mutation-dependent difference affecting V2R function. (pubmed_Id 19179480,16843086)
R143P	R143P and delta V278 mutants are retained within the cytoplasmic compartment. (pubmed_Id 7560098)
S167A	The mutant S167A was functionally active, (pubmed_Id 8863826)
R181C G185C	loss of receptor function (pubmed_Id 15841479)
G201D	the complex-glycosylated mutant G201D were partially located in lysosomes, G201D was expressed in the ER and in the basolateral membrane as immature, high-mannose glycosylated, and mature complex-glycosylated proteins. (pubmed_Id 18048502,16006591)
R202C	R202C mutant reaches the cell surface, a simple binding impairment at the cell surface (pubmed_Id 7560098)
T204N	degraded by only lysosomes, T204N was expressed in the ER and in the basolateral membrane as immature, high-mannose glycosylated, and mature complex-glycosylated protein (pubmed_Id 16006591)
Y205C Y205F Y205H	-for Y205C the lack of a Tyr residue at position 205 is responsible for the abolished receptor function rather than the formation of a disastrous second disulfide bond. Y205C mutant was almost inactive. -Analysis of the intermolecular interaction of the Tyr-205 hydrogen group by molecular modeling showed that Tyr-205 was located in transmembrane domain (TM) 5, and that its hydroxy group formed a hydrogen bond with Leu-169 main-chain =O located in TM 4. The mutation of Tyr-205 to phenylalanine would cause loss of this hydrogen bond and decrease or change the interaction between these TM coils, thus affecting the ability of AVP to bind to the receptor. According to this molecular model of AVPR2, the Y205F mutation would cause nephrogenic diabetes insipidus. - the loss of receptor function of Y205H, NDI-causing mutation Y205H which affects a codon frequently found to be mutated to Cys in NDI patients. (pubmed_Id 15841479,11026555, 17216256,)
V206D	stimulation of the V206D mutant increased the cAMP accumulation only slightly, V206D was mainly expressed in the endoplasmic reticulum (ER) as immature proteins. (pubmed_Id 11026555,16006591)

F287L	F287L mutant in COS-7 cells revealed significant dysfunction and accumulate intracellular cyclic adenosine monophosphate in response to AVP hormone stimulation. (pubmed_Id 11916004)
P322S	P322S mutation of AVPR2 gene leads to a mild form of CNDI. (pubmed_Id 10026830,9402087)
S363A	The S363A mutation that confers recycling to the V2R did not alter its interaction with arrestins. (pubmed_Id 11353798)

Table appendix: Overview of mutations in the V2 receptor and a short description of functional and structural influences.

8. References

Robertson GL (1995) Diabetes insipidus. *Endocrinol Metab Clin North Am* 24: 549-572.

Ananthakrishnan S (2009) Diabetes insipidus in pregnancy: etiology, evaluation, and management *Endocr Pract* 15: 377-382.

Krysiak, R.; Kobielusz-Gembala, I. et al (2010) Recurrent pregnancy-induced diabetes insipidus in a woman with hemochromatosis Endocrine Journal, online-ISSN: 1348-4540

Deen PM, Verdijk MA, Knoers NV, Wieringa B, Monnens LA, van Os CH, van Oost BA.Requirement of human renal water channel aquaporin-2 for vasopressin-dependent concentration of urine. *Science* 1994; 264: 92–95.

Mulders SM, Bichet DG, Rijss JPL, Kamsteeg EJ, Arthus MF, Lonergan M, Fujiwara M,

Morgan K, Leijendekker R, van der Sluijs P, van Os CH, Deen PMT. An aquaporin-2 water channel mutant which causes autosomal dominant nephrogenic diabetes insipidus is retained in the Golgi complex. *J Clin Invest* 1998; 102: 57–66.

Van den Ouweland AMW, Dreesen JCFM, Verdijk M, Knoers NVAM, Monnens LAH, Rocchi M, VanOost BA. Mutations in the vasopressin type-2 receptor gene (Avpr2) associated with nephrogenic diabetes-insipidus. *Nat Genet* 1992; 2: 99–102.

Rosenthal W, Seibold A, Antaramian A, Lonergan M, Arthus MF, Hendy GN, Birnbaumer M, Bichet DG. Molecular-identification of the gene responsible for congenital nephrogenic diabetes-insipidus. *Nature* 1992; 359: 233–235

Los, E. L .; Deen, P. M. T; Robben, J. H. Potential of Nonpeptide (Ant)agonists to Rescue Vasopressin V2 Receptor Mutants for the Treatment of X-linked Nephrogenic Diabetes Insipidus. *Journal of Neuroendocrinology* 2010; 22: 393–399

Fujiwara TM, Bichet DG. Molecular biology of hereditary diabetes insipidus. J AmSoc Nephrol. 2005;16:2836–46.

Robben JH, Knoers NVAM, Deen PMT. Cell biological aspects of the vasopressin type-2 receptor and aquaporin 2 water channel in nephrogenic diabetes insipidus. Am J Physiol Renal Physiol 2006; 291: F257–F270.

Hardy, C.; Khanim, F.; Torres, R. et al. Clinical and Molecular Genetic Analysis of 19 Wolfram Syndrome Kindreds Demonstrating a Wide Spectrum of Mutations in WFS1. Am. *J. Hum. Genet*. 1999; 65:1279–1290.

Wolfram, D.J. and Wagener, H.P. (1938) Diabetes mellitus and simple optic atrophy among siblings: report on four cases. *Mayo Clinic Proc.*,13, 715–718.

Swift, M. and Swift, R.G. (2001) Psychiatric disorders and mutations at the Wolfram syndrome locus. *Biol. Psychiatry*, 47, 787–793.

Strom, T.; Hörtnagel, K.; Hofmann, S. Diabetes insipidus, diabetes mellitus, optic atrophy and deafness (DIDMOAD) caused by mutations in a novel gene (wolframin) coding for a predicted transmembrane protein. *Human Molecular Genetics*, 1998, Vol. 7, No. 13: 2021–2028

Inoue, H., Tanizawa, Y., Wasson, J., Behn, P., Kalidas, K., Bernal-Mizrachi, E., Mueckler, M.,
Marshall, H., Donis-Keller, H., Crock, P. et al. (1998) A gene encoding a transmembrane protein is mutated in patients with diabetes mellitus and optic atrophy (Wolfram syndrome). *Nat. Genet*., 20, 143–148.

Strom, T.M., Hoetnagael, K., Hofmann, S., Gekeler, F., Scharfe, C., Rabl, W., Gerbitz, K.D. and Meitinger, T. (1998) Diabetes insipidus, diabetes mellitus, optic atrophy and deafness (DIDMOAD) caused by mutations in a novel gene (wilframin) coding for a predicted transmembrane protein. *Hum. Mol. Genet*., 7, 2021–2028.

Cryns, K., Sivakumaran, T.A., Van den Ouweland, J.M., Pennings, R.J., Cremers, C.W., Flothmann, K., Young, T.L., Smith, R.J., Lesperance, M.M. and Van Camp, G. (2003)
Mutational spectrum of the WFS1 gene in Wolfram syndrome, nonsyndromic hearing impairment, diabetes mellitus, and psychiatric disease. *Hum. Mut*., 22, 275–287.

Takeda, K., Inoue, H., Tanizawa, Y., Matsuzaki, Y., Oba, J., Watanabe, Y., Shinoda, K. and Oka, Y. (2001) WFS1 (Wolfram syndrome 1) gene product: predominant subcellular localization to endoplasmic reticulum in cultured cells and neuronal expression in rat brain. *Hum. Mol. Genet*., 10, 477–484.

Hofmann, S., Philbrook, C., Gerbitz, K.D. and Bauer, M.F. (2003) Wolfram syndrome: structural and functional analyses of mutant and wild-type wolframin, the WFS1 gene product. *Hum. Mol. Genet*., 12, 2003–2012.

King LS, Kozono D, Agre P. From structure to disease: the evolving tale ofaquaporin biology. *Nat Rev Mol Cell Biol*. 2004 5(9):687-98. Review.

Pollard TD, Earnshaw, WC. (2007), *Cell Biology*, Springer, ISBN 978-3-8274-1861-6, Heidelberg

Guyon C, Lussier Y, Bissonnette P, Leduc-Nadeau A, Lonergan M, Arthus MF, Perez RB, Tiulpakov A, Lapointe JY, Bichet DG. Characterization of D150E and G196D aquaporin-2 mutations responsible for nephrogenic diabetes insipidus: importance of a mild phenotype. *Am J Physiol Renal Physiol*. 2009;297(2):F489-98.

Ambrish Roy, Alper Kucukural and Yang Zhang, TASSER: a unified platform for automated protein structure and function prediction. *Nat Protoc*. 2010 April; 5(4): 725–738

D. Frenkel and B.J. Smit. Understanding Molecular Simulation. From Algorithms to Applications. Elsevier, 2002.

Jr. A. D. MacKerell, D. Bashford, M. Bellott, R. L. Dunbrack Jr., J. D. Evanseck, M. J. Field, S. Fischer, J. Gao, H. Guo, S. Ha, D. Joseph McCarthy, L. Kuchnir, K. Kuczera, F. T. K. Lau, C. Mattos, S. Michnick, T. Ngo, D. T. Nguyen, and B. Prodhom. All-atom empirical potential for molecular modeling and dynamics studies of proteins. *J. Phys. Chem. B*, 1998.

J. A. McCammon and M. Karplus. Internal motions of antibody molecules. *Nature*, 268(5622):765{766, Aug 1977.

Peter L. Freddolino, Anton S. Arkhipov, Steven B. Larson, Alexander McPherson, and Klaus Schulten. Molecular dynamics simulations of the complete satellite tobacco mosaic virus.*Structure*, 14:437-449, 2006.

Assembly of lipids and proteins into lipoprotein particles. Amy Y. Shih, Anton Arkhipov, Peter L. Freddolino, Stephen G. Sligar, and Klaus Schulten. Assembly of lipids and proteins into lipoprotein particles *Journal of Physical Chemistry B*, 111:11095-11104, 2007.

Yinglong Miao, Peter J. Ortoleva, Viral structural transition mechanisms revealed by multiscale molecular dynamics/order parameter extrapolation simulation. *Biopolymers* Volume 93, Issue 1, pages 61–73, January 2010Peter M. Kasson, Erik Lindahl, and Vijay S. Pande. Atomic-resolution simulations predict a transition state for *vesicle* fusion defined by contact of a few lipid. *PLoS Computational Biology*, *2010* June; 6(6): e1000829.

Jorgensen, W. L.; Chandrasekhar, J.; Madura, J. D.; Impey, R. W.; Klein, M. L. Comparison of simple potential functions for simulating liquid water. *J. Chem. Phys* 1983, *79*, 926-935.

James C. Phillips, Rosemary Braun Wei Wang James Gumbart, Emad Tajkhorshid, Elizabeth Villa, Christophe Chipot, Robert D. Skeel, Laxmikant Kalé, Klaus Schulten, Scalable molecular dynamics with NAMD

Barberis C, Mouillac B, Durroux T.,*J Endocrinol.* 1998 6(2):223-9. Structural bases of vasopressin/oxytocin receptor function.

Slusarz MJ, Giełdoń A, Slusarz R, Ciarkowski J. Analysis of interactions responsible for vasopressin binding to human neurohypophyseal hormone receptors-molecular dynamics study of the activated receptor-vasopressin-G(alpha) systems. *J Pept Sci*. 2006 Mar;12(3):180-9.

Feldman BJ, Rosenthal SM, Vargas GA, Fenwick RG, Huang EA, Matsuda-Abedini M, Lustig RH, Mathias RS, Portale AA, Miller WL, Gitelman SE.: Nephrogenic syndrome of inappropriate antidiuresis., N Engl J Med. 2005 352(18):1884-90.

Müller, D.J., Engel, A.: Voltage and pH-induced channel closure of porin OmpF visualized by atomic force microscopy. J. Mol. Biol. 285, 1347–1351 (1999)

Müller, D.J., Sass, H.J., Muller, S.A., Buldt, G., Engel, A.: Surface structures of native bacteriorhodopsin depend on the molecular packing arrangement in the membrane. *J. Mol.Biol*. 285, 1903–1909 (1999)

Seelert, H., Dencher, N.A., Muller, D.J.: Fourteen protomers compose the oligomer III of the proton-rotor in spinach chloroplast ATP synthase. *J. Mol. Biol*. 333, 337–344 (2003)

Janshoff, A., Neitzert, M., Oberdorfer, Y., Fuchs, H.: Force spectroscopy of molecular systems-single molecule spectroscopy of polymers and biomolecules. *Angew Chem. Int. Ed.* Engl. 39(18), 3212–3237 (2000)

Janovjak, H., Struckmeier, J., Hubain, M., Kedrov, A., Kessler, M., Muller, D.J.: Probing the energy landscape of the membrane protein bR. *Structure* 12(5), 871–879 (2004)

Rief, M., Gautel, M., Oesterhelt, F., Fernandez, J.M., Gaub, H.E.: Reversible unfolding of individual titin immunoglobulin domains by afm. *Science* 276(5315), 1109–1112 (1997)

Marsico A, Labudde D, Sapra T, Muller DJ, Schroeder M. A novel pattern recognition algorithm to classify membrane protein unfolding pathways with high-throughput single-molecule force spectroscopy. *Bioinformatics*. 2007

Sapra KT, Balasubramanian GP, Labudde D, Bowie JU, Muller DJ. Point mutations in membrane proteins reshape energy landscape and populate different unfolding pathways. *J Mol Biol*. 2008 Feb 29;376(4):1076-90.

Möller C, Fotiadis D, Suda K, Engel A, Kessler M, Müller DJ. Determining molecular forces that stabilize human aquaporin-1. *J Struct Biol*. 2003 Jun;142(3):369-78.

Chen H, Wu Y, Voth GA. Origins of proton transport behavior from selectivity domain mutations of the aquaporin-1 channel., *Biophys J.* 2006;90(10):L73-5.

de Groot, B. L., T. Frigato, V. Helms, and H. Grubmüller. 2003. The mechanism of proton exclusion in the aquaporin-1 water channel. *J. Mol. Biol.* 333:279–293.

Chakrabarti, N., E. Tajkhorshid, B. Roux, and R. Pomes. 2004. Molecular basis of proton blockage in aquaporins. *Structure.* 12:65–74.

Chakrabarti, N., B. Roux, and R. Pome`s. 2004. Structural determinants of proton blockage in aquaporins. *J. Mol. Biol.* 343:493–510.

Ilan, B., E. Tajkhorshid, K. Schulten, and G. A. Voth. 2004. The mechanism of proton exclusion in aquaporin channel. *Proteins*. 55: 223–228.

Dressel, F., Tuukkanen, A., Schroeder M., and Labudde, D., Understanding of SMFS barriers by means of energy profiles, *Proc. GCB*, 2007

Wertz, D. H. and Scheraga, H. A., Influence of water on protein structure. An Analysis of the preferences of amino acid residues for the inside or outside and for specific conformations in a protein molecule. *Macromolecules*. 1978 Jan-Feb;11(1):9-15.

Gusfield D., Efficient Methods for Multiple Sequence Alignment with Guaranteed Error Bounds, *Bulletin of Mathematical Biology*, Vol. 55, p. 141-154, 1993

Gusfield D., Algorithms on Strings, Trees and Sequences, Cambridge University Press, 1997

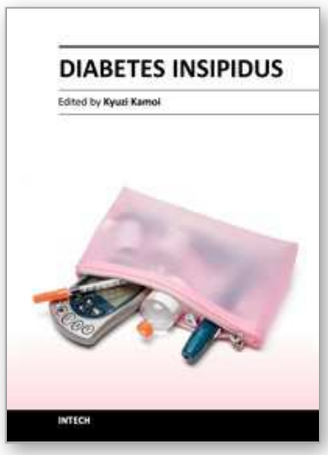

Diabetes Insipidus

Edited by Prof. Kyuzi Kamoi

ISBN 978-953-307-367-5
Hard cover, 140 pages
Publisher InTech
Published online 14, November, 2011
Published in print edition November, 2011

The first chapter of the book reports on the management of Langerhans cell histiocytosis (LCH)-induced central diabetes insipidus and its associated endocrinological/neurological sequelae in the national survey. The next chapter addresses DI and head injuries. Next, the management of neuroendocrine instability during maintenance of potential organ donors is described. Organ transplants have gradually increased worldwide. To have maintenance of appropriate potential organs, AVP is needed. Furthermore, nephrogenic DI-the potential therapeutic drugs and analysis of membrane protein stability is the topic of the next two chapters, followed by new insights into the diagnosis and management of pregnancy-related DI. The seventh chapter reports on the problems with differential diagnosis in a case of central DI in a female patient with bipolar disorder. The lithium treatment usually resulted in nephrogenic DI. Finally, over the last years, the development of MRI imaging on the pituitary gland with the stalk and hypothalamus has advanced. The final chapter interprets imaging techniques in DI in detail.

InTech Europe
University Campus STeP Ri
Slavka Krautzeka 83/A
51000 Rijeka, Croatia
Phone: +385 (51) 770 447
Fax: +385 (51) 686 166
www.intechopen.com

InTech China
Unit 405, Office Block, Hotel Equatorial Shanghai
No.65, Yan An Road (West), Shanghai, 200040, China
中国上海市延安西路65号上海国际贵都大饭店办公楼405单元
Phone: +86-21-62489820
Fax: +86-21-62489821

IntechOpen